ADVANCED MATERIALS
www.advmat.de

Photoelectrochemical N_2-to-NH_3 Fixation with High Efficiency and Rates via Optimized Si-Based System at Positive Potential versus $Li^{0/+}$

Xiaoran Zhang, Yanhong Lyu, Huaijuan Zhou, Jianyun Zheng, Aibin Huang, Jingjing Ding, Chao Xie, Roland De Marco, Nataliya Tsud, Viacheslav Kalinovych, San Ping Jiang,* Liming Dai, and Shuangyin Wang**

As a widely used commodity chemical, ammonia is critical for producing nitrogen-containing fertilizers and serving as the promising zero-carbon energy carrier. Photoelectrochemical nitrogen reduction reaction (PEC NRR) can provide a solar-powered green and sustainable route for synthesis of ammonia (NH_3). Herein, an optimum PEC system is reported with an Si-based hierarchically-structured PdCu/TiO_2/Si photocathode and well-thought-out trifluoroethanol as the proton source for lithium-mediated PEC NRR, achieving a record high NH_3 yield of 43.09 μg cm^{-2} h^{-1} and an excellent faradaic efficiency of 46.15% under 0.12 MPa O_2 and 3.88 MPa N_2 at 0.07 V versus lithium(0/+) redox couple (vs $Li^{0/+}$). PEC measurements coupled with operando characterization reveal that the PdCu/TiO_2/Si photocathode under N_2 pressures facilitate the reduction of N_2 to form lithium nitride (Li_3N), which reacts with active protons to produce NH_3 while releasing the Li^+ to reinitiate the cycle of the PEC NRR. The Li-mediated PEC NRR process is further enhanced by introducing small amount of O_2 or CO_2 under pressure by accelerating the decomposition of Li_3N. For the first time, this work provides mechanistic understanding of the lithium-mediated PEC NRR process and opens new avenues for efficient solar-powered green conversion of N_2-to-NH_3.

1. Introduction

As one of the world's most important chemicals, ammonia (NH_3) is an indispensable feedstock for fertilizer.[1,2] Current industrial production of NH_3 is predominantly via the century-old Haber–Bosch process to react nitrogen (N_2) with hydrogen (H_2) over heterogeneous catalysts at high temperatures of 450–500 °C and pressures up to 20 MPa, leading to about 2% of the world's energy consumption and 1.5% of total global CO_2 emissions.[3,4] To overcome the energy and environmental challenges associated with the Haber–Bosch process, a photoelectrochemical nitrogen reduction reaction (PEC NRR) route has been demonstrated to produce NH_3 from N_2 and sun-light in aqueous electrolytes at ambient conditions.[5–7] Various photocathodes have been fabricated through heteroatom doping,[8]

X. Zhang, Y. Lyu, J. Zheng, J. Ding, C. Xie, S. Wang
State Key Laboratory of Chem/Bio-Sensing and Chemometrics
College of Chemistry and Chemical Engineering
Hunan University
Changsha 410082, P. R. China
E-mail: jyzheng@hnu.edu.cn; shuangyinwang@hnu.edu.cn

X. Zhang, S. P. Jiang
Foshan Xianhu Laboratory of the Advanced Energy Science and Technology Guangdong Laboratory
Foshan 528216, China
E-mail: S.Jiang@curtin.edu.au

H. Zhou
Advanced Research Institute of Multidisciplinary Sciences
Beijing Institute of Technology
Beijing 100081, China

The ORCID identification number(s) for the author(s) of this article can be found under https://doi.org/10.1002/adma.202211894.

DOI: 10.1002/adma.202211894

A. Huang
State Key Laboratory of High Performance Ceramics and Superfine Microstructure
Shanghai Institute of Ceramics
Chinese Academy of Sciences
Shanghai 200050, China

A. Huang
Center of Materials Science and Optoelectronics Engineering
University of Chinese Academy of Sciences
Beijing 100049, China

R. De Marco
School of Chemistry and Molecular Biosciences
The University of Queensland
Brisbane, QLD 4072, Australia

R. De Marco
Department of Chemistry
School of Pure Science
College of Engineering
Science and Technology
Fiji National University
Samabula, P.O. Box 3722, Suva, Fiji

defect engineering,[9,10] and surface/interface engineering[11,12] for producing variable quantities of NH_3 from N_2 in aqueous electrolytes. Of particular interest, Yan's group used a salting-out effect from a highly concentrated aqueous electrolyte to enhance the performance of NRR by reducing the competing hydrogen evolution and increasing the N_2 accessibility.[13] Meanwhile, others have effectively moved the chemical equilibrium towards the NH_3 formation by increasing N_2 solubility under pressure[14] and accelerated the N_2 activation and hydrogenation through multistep reactions.[15] Although the great potential of PEC NRR has attracted worldwide research activities, its practical implementation is still severely limited by the low NH_3 production rate (usually < 10 μg cm^{-2} h^{-1}) and poor faradaic efficiency (FE, typically <30%).[6]

Apart from the aqueous electrolytes, lithium (Li)-containing non-aqueous electrolytes have also been used for electrochemical NRR to enhance the NH_3 yield.[16] In this Li-mediated NRR mode, lithium ions (Li^+) are reduced to metal Li (the standard redox potential of $Li/Li^{0/+}$ is −3.04 V vs standard hydrogen electrode, SHE), which can spontaneously react with N_2 to form lithium nitride (Li_3N) and then capture active protons to form NH_3, as shown below[17]

$$3Li^+ + \frac{1}{2}N_2 \overset{3e^-}{\leftrightarrows} Li_3N \overset{3H^+}{\rightarrow} 3Li^+ + NH_3 \quad (1)$$

Great progress has been made from intensive research on the electrochemical Li-mediated NRR,[18,19] and a record high NH_3 yield rate of 150 nmol cm^{-2} s^{-1} with an almost 100% FE was achieved recently by using a high-concentration bis(trifluoromethylsulfonyl)imide lithium ($LiNTf_2$) under 1.5 MPa N_2 at −0.55 V versus lithium(0/+) redox couple (vs $Li^{0/+}$).[20] Different to the conventional electrochemical method, Li-mediated PEC NRR could occur at a positive potential versus $Li^{0/+}$ under sunlight to reduce the external energy consumption. However, Li-mediated PEC NRR is rarely studied and there is no fundamental understanding of its catalytic mechanism, and hence the lack of know how to rationally improve the process.

Herein, we for the first time demonstrated the Li-mediated PEC NRR by using silicon (Si)-based hierarchical photocathodes in a $LiClO_4$-propylene carbonate (PC) solution at optimized reaction conditions to obtain a high NH_3 yield rate of 43.09 μg cm^{-2} h^{-1} and excellent faradic efficiency of 46.15% at 0.07 V versus $Li^{0/+}$. Lithium perchlorate ($LiClO_4$) was used as the electrolytes for Li-mediated PEC NRR due to its high stability, safety and free labile N-containing group.[21,22] Comprehensive PEC measurements coupled with operando characterization indicate that the Li-mediated PEC NRR is controlled by two main rate-limiting steps: (1) photoelectrons generated by the Si-based photocathode facilitate the metallic Li to reduce N_2 to form lithium nitride (Li_3N), followed by reacting with active protons to produce NH_3; and (2) the decomposition of Li_3N to release Li^+ to reinitiate the cycle of PEC NRR. As we shall see later, the mechanistic understanding enables us to improve the performance for the Li-mediated PEC NRR by optimizing different factors that influence the NRR reaction, including N_2 pressure, applied potential, chemical nature of the proton source, and reaction conditions. To the best of our knowledge, this is the first report to point out the importance of the Li/Li_3N cycle in the Li-mediated PEC NRR and provide an efficient route for the production of NH_3 at a positive potential versus $Li^{0/+}$ under sunlight to reduce the external energy consumption.

2. Results and Discussion

2.1. Synthesis and Characterization of Si-Based Hierarchical-Structured Photocathodes

Photocathode that provides actives sites for absorption, activation and hydrogenation of N_2 as well as desorption of the newly-formed NH_3 is the core component of a PEC NRR cell. Based on our previous work,[11,23] we used PdCu alloy, thin TiO_2 layer, and nanostructured Si-based wafer as the cocatalyst, protection layer and light absorber, respectively, to devise a Si-based hierarchically-structured photocathode for the Li-mediated PEC NRR in this study. Figure S1 (Supporting Information) schematically shows the process for fabricating the hierarchical Si-based photocathode, involving the following three main steps: (1) the preparation of nanostructured n^+p-Si absorber; (2) the deposition of a TiO_2 protection layer; and (3) the incorporation of the PdCu alloy cocatalyst. The preparation details for a $PdCu/TiO_2/Si$ photocathode are described in the Experimental Section of Supporting Information.

Field emission scanning electron microscopy (FESEM) with line-scanning energy dispersive spectroscopy (EDS) was used to reveal the architecture of the Si-based photocathode. **Figure 1**a,b clearly shows a hierarchical structure with a PdCu cocatalyst layer of ≈50 nm and TiO_2 protection layer of ≈25 nm in $PdCu/TiO_2/Si$ photocathode. The Pd and Cu elemental distributions shown in Figure 1b nearly coincided each other, implying the formation of the PdCu alloy.[24] PdCu alloy nanoparticles smaller than 10 nm aggregated and stacked on the top of the photocathode (Figure S2a,b, Supporting Information), in consistence with atomic force microscopy (AFM) images (Figure S3, Supporting Information). In addition, the stacked PdCu nanoparticles resulted in the formation of the porous PdCu cocatalyst layer (Figure S2b, Supporting Information), which can increase the active sites and allow the light to pass through the layer. As shown in Figure 1c and Figure S4a (Supporting Information), although $PdCu/TiO_2/Si$ showed a higher light reflection (less than 15%) than black Si (near-zero reflection) and TiO_2/Si (less than 10%), the hierarchical photocathode with porous PdCu layer can trap and absorb a large proportion of incident

N. Tsud, V. Kalinovych
Charles University
Faculty of Mathematics and Physics
Department of Surface and Plasma Science
Holešovičkách 2, Prague 18000, Czech Republic
S. P. Jiang
WA School of Mines: Minerals
Energy and Chemical Engineering
Curtin University
Perth, WA 6102, Australia
L. Dai
Australian Carbon Materials Centre (A-CMC)
School of Chemical Engineering
University of New South Wales
Sydney, NSW 2052, Australia

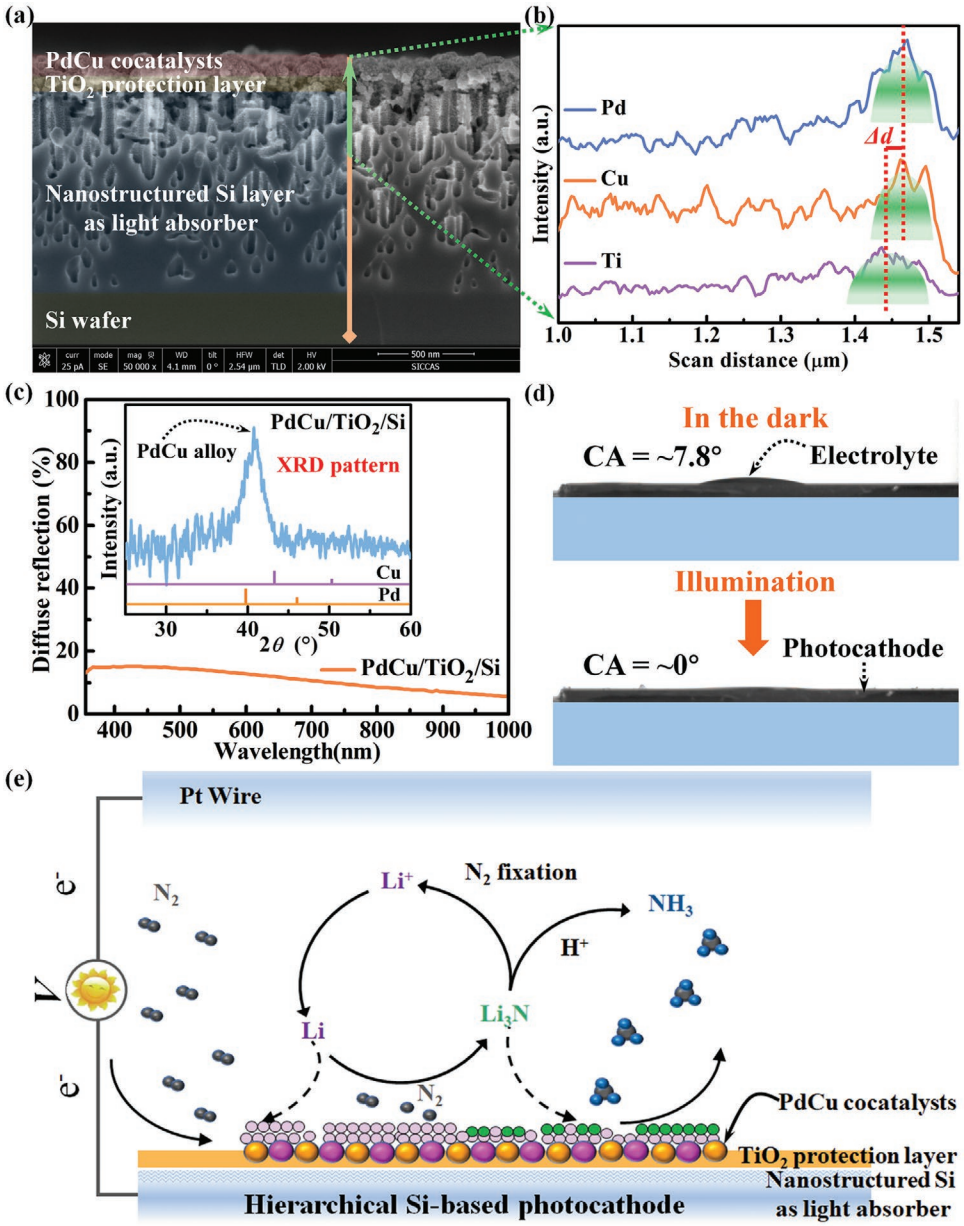

Figure 1. Chemical and physical characterizations of the hierarchical Si-based photocathode. a) Cross-sectional FESEM image of PdCu/TiO_2/Si, in which PdCu alloy, thin TiO_2 layer, and nanostructured Si-based wafer function as the cocatalyst, protection layer and light absorber, respectively. b) Corresponding line-scanning EDS curves of Pd, Cu, and Ti element. c) The measured total hemispherical optical reflectance of PdCu/TiO_2/Si in air. The inset shows XRD pattern of the photocathode. d) Photographs of the liquid droplets on the surface of PdCu/TiO_2/Si before and after irradiation for 30 min. e) Schematic illustration of Li-mediated PEC NRR on PdCu/TiO_2/Si.

light. Due to the presence of nanostructured Si, the Si-based hierarchical photocathode exhibited a low reflectance over 350–1000 nm (Figure 1c; Figure S4a, Supporting Information) with a bandgap of 1.1 eV determined by the optical absorption derived from the reflectance spectrum (Figure S4b, Supporting Information).[25] In addition, the crystalline structure of the photocathode was detected by grazing incidence X-ray diffraction (GIXRD). As shown in the inset of Figure 1c, the PdCu/TiO_2/Si exhibited a weak and broad XRD peak at 40.8° attributable to (111) plane of the PdCu alloy with no peak corresponding to the TiO_2 phase, indicating that the TiO_2 protection layer is amorphous. Also, there is no localized surface plasmon resonance (LSPR) resonance peak found in the optical measurements (see Figure 1c; Figure S4, Supporting Information). To further understand the LSPR effect of PdCu cocatalysts and testify the role of Si as light absorber, the PEC behaviors of PdCu/TiO_2 sample was carried out. The results show that there is no visible change by turning on/off the light. This can be attributed to the presence of Cu–O bonds and Pd–O bonds on the surface of PdCu cocatalysts (see below SR-XPS results). Thus, the contribution of LSPR effect from PdCu cocatalysts is negligible in this case.

To investigate Li^+ adsorption on the photocathode, we put a droplet of the 1 M $LiClO_4$-PC solution on the PdCu/TiO_2/Si surface before and after light illumination. Compared to that in the dark, the illuminated PdCu/TiO_2/Si displayed a more lyophilic surface with a contact angle (CA) of ≈0°, namely super-lyophile. As such, we anticipate that PdCu/TiO_2/Si can actively catalyze the Li-mediated PEC NRR process. As schematically illustrated in Figure 1e, the photoinduced electrons form the nanostructured Si layer upon illumination transport through the TiO_2 protection layer to the PdCu cocatalyst, reducing Li^+ ions into Li metal on the photocathode surface as the SEI layer to react with N_2 for the formation of Li_3N. The resultant Li_3N with a very strong base is readily protonated by proton sources (e.g., ethanol (EtOH)), producing NH_3 and at the same time releasing the Li^+ ions into the next reaction cycle (Figure 1e). Meanwhile, the photoinduced holes transport through the external circuit to the platinum (Pt) counter electrode to oxidize the proton source.

The performance of the Li-mediated PEC NRR process for the Si-based hierarchically-structured PdCu/TiO_2/Si photocathode was first assessed in 1 M $LiClO_4$-PC with 3% EtOH at different applied potentials versus $Li^{0/+}$ and N_2 pressures under 1 sun, using a gas-tight reactor with a liquid-seal cell (Figure S5, Supporting Information). The indophenol blue method, supplemented by nuclear magnetic resonance (NMR) measurements, was adopted to determine the NH_3 yield from the Li-mediated PEC NRR (see the Experimental Section in the Supporting Information).[14,26] Specifically, Figure S6 (Supporting Information) shows a standard calibration curve (Figure S6b, Supporting Information) derived from Figure S6a (Supporting Information) by plotting the optical absorbance at 650 nm as a function of the NH_4^+ ion concentration. To exclude possible false positive resulting from labile N-containing contamination, we first performed three necessary control experiments as follows: (1) measurements under open-circuit voltage, without the photocathodes, and in the dark were carried out (Figures S7–S9, Supporting Information). For example, using PdCu/TiO_2/Si photocathodes at 0.82 to –0.43 V versus $Li^{0/+}$ in the dark for 4 h, the photocathodes showed extremely low current densities due to lack of the photogenerated charge carriers (Figure S9, Supporting Information). In all cases, no NH_3 generation was detected in the electrolytes after 4 h-electrolysis as shown by the indophenol blue method; (2) no NH_3 (below the determination limit of 0.1 μg mL^{-1}) was detected in the electrolyte with argon (Ar) as the feeding gas for the PEC reaction (Figure S10, Supporting Information), indicating that the 1 M $LiClO_4$-PC electrolyte used is free from contaminates (e.g., nitrate, Figure S11, Supporting Information); and (3) $^{15}N_2$ isotope-NMR experiments were performed to confirm the N_2 feeding gas as the N sources for the PEC NRR production of NH_3 – no triple peak from $^{14}NH_4^+$ was observed when $^{15}N_2$ was used as the feeding gas (Figure S12, Supporting Information).

Having checked and avoided the possible false positive results from labile N-containing contamination, we carried out the performance evaluation of the Li-mediated PEC NRR for the Si-based hierarchically-structured PdCu/TiO_2/Si photocathode at different applied potentials. Figure S13 (Supporting Information) reproduces the linear sweep voltammetry (LSV) curves for the PdCu/TiO_2/Si photocathode, which shows strong and repeatable photocurrent responses in the N_2-saturated electrolyte at ambient conditions under illumination, but not in the dark, confirming the occurrence of the PEC reaction. **Figure 2**a shows the NH_3 yield rate and FE for PdCu/TiO_2/Si and TiO_2/Si

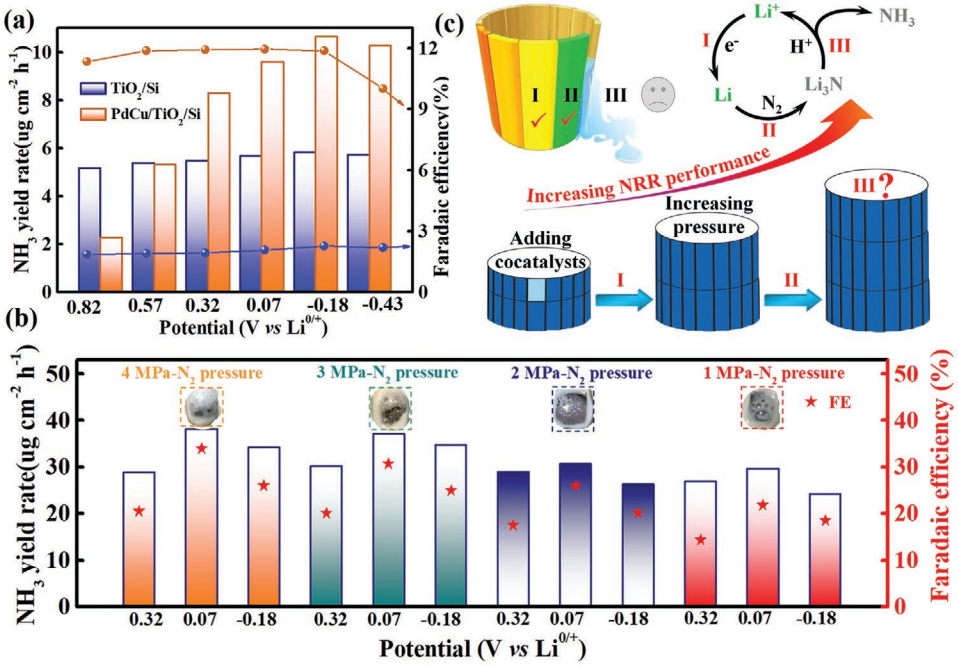

Figure 2. Li-mediated PEC NRR performance of Si-based photocathodes in 1 M $LiClO_4$-PC with 3% EtOH for 4 h under 1 sun. a) NH_3 yield rate (column diagram) and FE (point plot) of PdCu/TiO_2/Si (orange) and TiO_2/Si (blue) at various applied potentials versus $Li^{0/+}$ under ambient conditions. b) NH_3 yield rate (column diagram) and FE (star symbol) acquired from PdCu/TiO_2/Si as a function of N_2 pressures. c) Diagrammatic sketch for the proposed reaction steps and critical issues of Li-mediated PEC NRR.

photocathodes at different applied potentials under ambient conditions. Compared to the TiO_2/Si control photocathode, PdCu/TiO_2/Si photocathode displayed a much better performance for the Li-mediated PEC NRR with a higher NH_3 yield rate and FE. The main function of a thin and amorphous TiO_2 layer on the surface of nanostructured n^+p-Si absorber is to serve as an adhesion layer for growing the PdCu alloy cocatalysts and increase the stability during PEC NRR process and rather than to enhance the PEC performance, as shown in this study. Specifically, at the applied potential of –0.18 V versus $Li^{0/+}$ (corresponding to –3.22 V vs SHE), the PdCu/TiO_2/Si photocathode achieved the highest NH_3 yield rate of ≈10.63 μg cm^{-2} h^{-1} and FE of 11.96% under N_2 bubbles (flow rate of 30 sccm) and at an ambient pressure (Figure 2a). Beyond this negative potential, the NH_3 yield rate and FE on the photocathode decreased, which can be attributed to the presence of competitive reactions (e.g., Li extraction). In a separate study of Li extraction, we also observed the formation of clear and thick Li layer on the surface of photocathode during the PEC tests and the formation of thick metallic Li layer would block the light and affect the light absorption and harvesting. As a result, the addition of the PdCu cocatalyst facilitated the adsorption and reduction of Li^+ and the formation of the Li SEI layer, and hence the improved Li-mediated performance for the PdCu/TiO_2/Si photocathode. However, it is noted that the above observed Li-mediated PEC NRR performance in the $LiClO_4$ electrolyte is still lower than those reported for selected Li-mediated electrochemical NRR processes (Table S1, Supporting Information). The reason is most likely due to the low N_2 solubility in the electrolyte under ambient pressure, which could limit the formation rate of Li_3N and influence the NH_3 yield rate and current-to-NH_3 conversion efficiency, as demonstrated earlier.[27]

To overcome the N_2 solubility limitation, we further used a pressurized reactor to study the Li-mediated PEC NRR on the PdCu/TiO_2/Si photocathode under different N_2 pressures (N_2 was bubbled into the cell for 30 min to purge other gases, e.g., O_2, before introducing the target N_2 pressures) for 4 h within a closed and static PEC reaction environment (Figure S14, Supporting Information). A positive correlation between the N_2 pressure and the Li-mediated PEC NRR performance was observed, as shown in Figure 2b. Upon increasing the N_2 pressure from one atmosphere to 1 MPa, the applied potential for the best PEC NRR performance shifted from –0.18 (Figure 2a) to 0.07 V versus $Li^{0/+}$, in accordance with the Le Chatelier's principle about the movement of chemical equilibrium.[28] An NH_3 yield rate of 36.98 μg cm^{-2} h^{-1} and FE of 30.66% were achieved under the N_2 pressure of 3 MPa at 0.07 V versus $Li^{0/+}$ (corresponding to –2.97 V vs SHE), leading to ≈3.5- and 2.6-fold enhancements in the NH_3 yield rate and FE, respectively, for the same PdCu/TiO_2/Si photocathode at ambient pressure. Further increasing the N_2 pressure up to 4 MPa caused a small enhancement in the Li-mediated PEC NRR performance for the PdCu/TiO_2/Si photocathode with a NH_3 yield rate of 38.09 μg cm^{-2} h^{-1} and FE of 33.87% (Figure 2b). These results indicate that the pressurization-induced enhancement in N_2 solubility and N_2 delivery could facilitate the production of abundant Li_3N and ameliorate the rate-determining step (RDS) of $6Li + N_2 \rightarrow 2Li_3N$ for the Li-mediated NRR.[29] When the N_2 pressure is over 3 MPa, however, the N_2 solubility in the electrolyte would be sufficiently high to produce the saturated number of Li_3N sites on the surface of the PdCu/TiO_2/Si photocathode. Under this circumstance, the performance of the Li-mediated PEC NRR could be impeded by other reaction steps (such as the decomposition of Li_3N) rather than the transformation step from Li to Li_3N (as schematically shown in Figure 2c).

To probe changes in the chemical state and electron structure of the photocathode surface in the dark and under illumination, we performed operando synchrotron radiation X-ray photoelectron spectroscopy (SR-XPS) for the Si-based hierarchically-structured PdCu/TiO_2/Si photocathode during the Li-mediated PEC NRR.[30] As shown in the lower curve of **Figure 3**a, the Cu 2p spectrum of PdCu/TiO_2/Si in the dark can be fitted into five peaks, consisting of two Cu $2p_{3/2}$ peaks, two Cu $2p_{1/2}$ peaks and one satellite peak. Notably, the two peaks of Cu $2p_{3/2}$ centered at 932.1 and 934.3 eV are associated with Cu–Cu and Cu–O bonds, respectively.[31] In the dark, the average metallic state of Cu (as defined by the peak area ratio of M–M to M–O; M = Cu or Pd) on PdCu/TiO_2/Si is about 0.95, implying that Cu on the photocathode surface can be readily oxidized by the ambient O_2 due to the high surface Gibbs free energy intrinsically associated with the nanoparticles.[32] Upon irradiation, the Cu–Cu peak shifted to a lower binding energy of 931.7 eV (see the top curve of Figure 3a) from 932.1 eV measured in the dark with a concomitant increase in the average metallic state of Cu from 0.95 to ≈1.49, while there was no obvious change in the peak position for the Cu–O bond. The corresponding Pd 3d spectra in Figure 3b show two Pd $3d_{7/2}$ peaks at ≈335.7 and 336.7 eV characteristic of the Pd–Pd and Pd–O bonds, respectively.[33] Similar to the Cu 2p spectra in Figure 3a, the illumination also caused a downward shift to a lower binding energy of 335.4 eV for the Pd–Pd peak and a slight increase in the ratio of Pd–Pd to Pd–O from 2.89 to 3.18 (Figure 3b). These results indicate the photoinduced charge generation and separation, followed by the electron transport from the nanostructured optical absorber of n^+p-Si to the PdCu alloyed nanoparticles. The resultant electron-rich Pd and Cu sites could serve as the Lewis base to facilitate the adsorption and reduction of the Li^+ to Li on the surface of the PdCu/TiO_2/Si photocathode.

To gain insights on the underlying mechanism associated with the Li chemical state changes, we further performed Quasi in situ GIXRD measurements to collect information about the phase structure and chemical composition of the photocathode surface after the Li-mediated PEC NRR. As shown in Figure 3c, there is no remarkable peak observed in the diffraction angle range from 28° to 34° prior to the PEC NRR process. During the initial reaction stage (e.g., >1 h), a small peak appeared around ≈32.9°, which can be assigned to the Li_2O phase[34,35] resulted from the oxidation of Li or Li_3N with the ambient air, in line with the phenomenon that the white layer on the surface of post-electrolysis PdCu/TiO_2/Si photocathode reacted violently in the air to yield the fizziness (Figure S15, Supporting Information). The Li_2O peak intensity increased with increasing reaction time (Figure 3c). After about 1.5-h electrolysis, a new weak peak at ~31.5° characteristic of the Li_3N phase[36,37] appeared, which is accompanied by the appearance of a strong peak at ≈29.6° corresponding to $Li_2N_2O_3$ as the intermediate from the Li_3N oxidation under ambient.[38,39] These results provide strong evidences for the successful synthesis

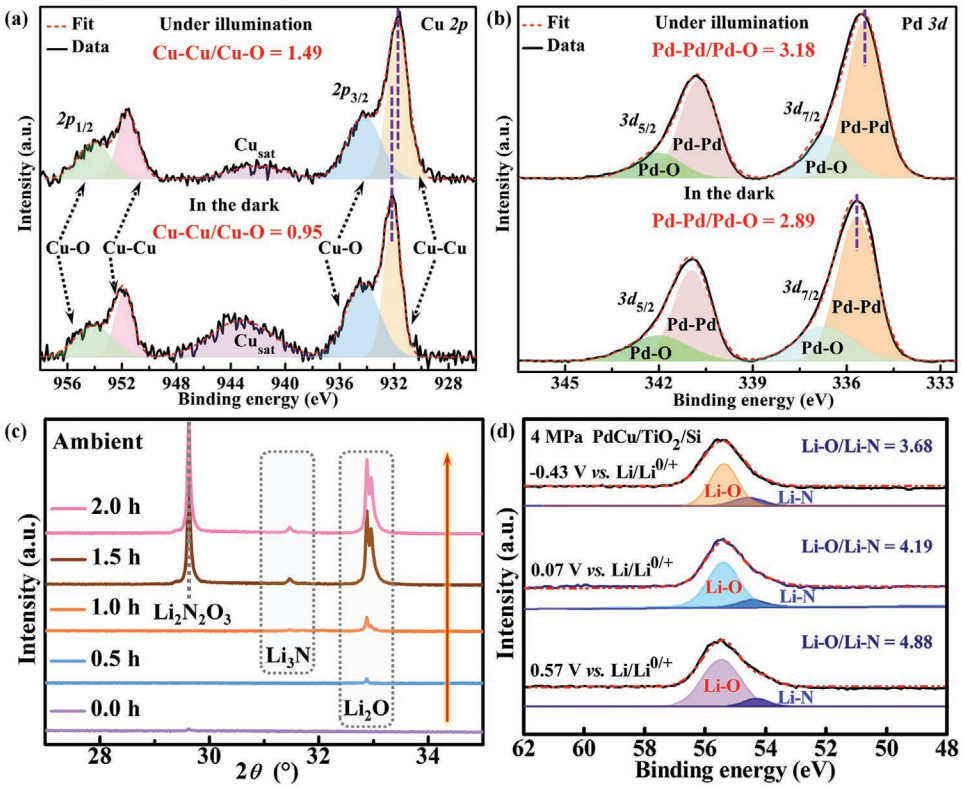

Figure 3. Analysis of active sites on the hierarchical Si-based photocathode and work mechanism on the formation of Li and Li_3N by various operando characterizations. a) Cu 2p and b) Pd 3d of PdCu/TiO_2/Si using SR-XPS in the dark and under illumination. The light sources with 520 nm using in (a) and (b) were yielded by a low-powered laser product (≈0.1 mW output power). c) XRD patterns of PdCu/TiO_2/Si obtained after Li-mediated PEC NRR at –0.18 V versus $Li^{0/+}$ with different reaction time. d) Li 1s of XPS spectra for the reacted PdCu/TiO_2/Si at given applied potentials under 4-MPa N_2 pressure and 1 sun.

of Li_3N from Li and N_2 during the PEC NRR process, and also indicate a higher stability for Li_3N and $Li_2N_2O_3$ in air than that of Li (Figure 3c). Along with the quasi in situ XRD measurements, quasi in situ Raman spectra (Figure S16, Supporting Information) were also obtained to show Raman modes for the Li_3N over 400–500 cm^{-1}.[40,41]

To further reveal electronic states and chemical bonds of the Li species, we measured Li 1s XPS spectra for the reacted PdCu/TiO_2/Si after the Li-mediated PEC NRR under 4-MPa N_2 for 4 h at different applied potentials (Figure 3d). The obtained Li 1s XPS spectra of the PdCu/TiO_2/Si photocathode electrolyzed at all the applied potentials were deconvolved into two peaks at 55.5 and 54.2 eV attributable to the Li–O and Li–N bonds, respectively,[42,43] according to the Lorentzian-Gaussian distribution function. The curve-fitted Li 1s XPS spectra in Figure 3d clearly show the formation of Li_3N during the PEC NRR process, in consistence with the quasi in situ XRD and Raman measurements. A decrease in the applied potential from 0.57 to –0.43 V versus $Li^{0/+}$ led to a continuous decrease in the ratio of Li–O to Li–N from 4.88 to 3.68. These results, together with the irregular relationship between the EF and applied potential shown in Figure 2b, indicate that the Li-mediated PEC NRR performance of the PdCu/TiO_2/Si photocathode is not simply proportional to the variations in the content of Li_3N on the photocathode surface. Thus, there is an optimal content of the Li_3N for the Li-mediated PEC NRR process. This is because when the Li_3N content is less than the optimal value, the formation of Li_3N is the rate-limiting step for the Li-mediated PEC NRR process. When an excessive amount of Li_3N accumulate on the photocathode surface, however, the interface resistance increases to impede the Li cycle (Figure 2c), leading to the performance decay for the Li-mediated PEC NRR.

The important role of Li_3N in regulating the Li-mediated PEC NRR performance was further investigated. On the basis of Equation 1, we can envision that the accumulation of Li_3N could be related to the sluggish rate for hydrogenation of the Li_3N to produce NH_3 via $Li_3N + 3MH \rightarrow 3Li^+ + 3M^- + NH_3$ (M is the functional group). To validate this hypothesis, we used proton sources with different H^+ donating capabilities in the electrolytes to control the hydrogenation of Li_3N for the Li-mediated PEC NRR performance. The proton sources used in this work include isopropyl alcohol (IPA), methanol (MeOH), ethanol (EtOH), and trifluoroethanol (TFE) with the H^+ donating capability (namely, the Bronsted acidity) in the order of TFE > MeOH > EtOH > IPA. As shown in **Figure 4**a, the Bronsted acidity of the proton donors significantly affects the pressurized (e.g., 4-MPa N_2 pressure) Li-mediated PEC NRR performance. Specifically, the NH_3 yield rate and FE of the PEC NRR gradually increased with increasing the Bronsted acidity of the proton donors. When TFE was used as the proton donor, the NH_3 yield rate and FE for the Li-mediated PEC NRR were 38.12 μg cm^{-2} h^{-1} and 40.66%, respectively, which

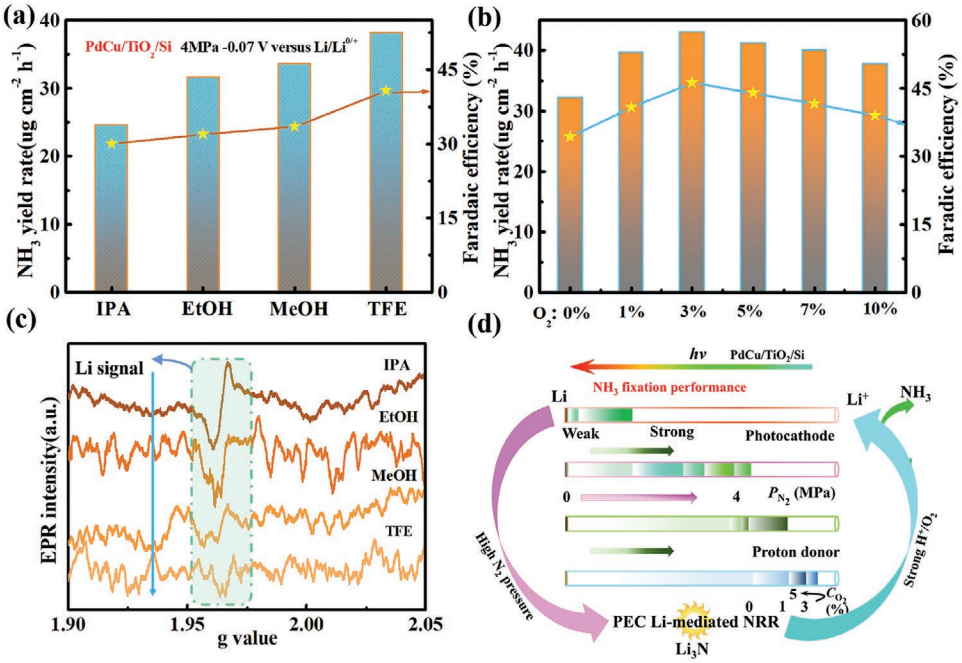

Figure 4. Effect of proton sources and gas composition on the synthesis of NH_3 and the completely enhanced mechanism of Li-mediated PEC NRR. a) NH_3 yield rate (column diagrams) and FE (point plots) from Li-mediated PEC NRR as a function of proton sources under condition of 1 sun, 4-MPa N_2 and 0.07 V versus $Li^{0/+}$. b) The dependence of NRR performance on the O_2 concentrations of mixed N_2/O_2 gas under 1 sun and 0.07 V versus $Li^{0/+}$. c) Quasi in situ EPR spectra of the post-electrolysis photocathode under condition of 4-MPa N_2 and 0.07 V versus $Li^{0/+}$ with the electrolytes containing different proton sources. d) Schematic representation of the completely enhanced mechanism of Li-mediated PEC NRR system by optimizing the process of Li cycle.

are 1.55 and 1.36 times higher than the corresponding values for IPA as the proton donor (Figure 4a). The LSV curves of the $PdCu/TiO_2/Si$ photocathode in the N_2-saturated electrolyte with TFE proton sources at ambient conditions under illumination show strong and repeatable photocurrent responses (Figure S17, Supporting Information). Therefore, the proton donor with a strong Bronsted acidity has a tendency to capture the Li site of Li_3N and cause the rupture of the Li–N bonds to accelerate the NH_3 formation. The electrochemical impedance spectroscopy (EIS, see Figure S18 in the Supporting Information) results demonstrated that the addition of different proton sources in electrolyte can tune the charge transfer resistance (R_{ct}) of the photocathode surface. The order of charge transfer resistance for $PdCu/TiO_2/Si$ photocathode is $LiClO_4$+TFE < $LiClO_4$+MeOH < $LiClO_4$+EtOH < $LiClO_4$+IPA, in line with the corresponding Li-mediated PEC NRR performance.

As pointed out by Li et al., the addition of O_2 improves the FE of Li-mediated electrocatalytic NRR.[44] Nevertheless, the work mechanism of O_2 in the NRR behavior or Li cycle is not clear. In view of the air-oxidation of Li_3N to form the unstable intermediate to weaken the Li–N bond discussed above, we also introduced an appropriate amount of O_2 into the Li-mediated PEC NRR cell to try to facilitate the decomposition of Li_3N. Figure 4b shows the dependence of the PEC NRR performance on the O_2 concentration in a N_2/O_2 mixture gas under 1 sun at 0.07 V versus $Li^{0/+}$. The best performance of the Li-mediated PEC NRR was obtained at an O_2 concentration of 3%, achieving an NH_3 yield rate of 43.09 μg cm^{-2} h^{-1} and FE of 46.15%. The NRR performance decreased as the O_2 concentration was over 3% due to the production of stable Li_2O to reduce the Li_3N species. Similar phenomenon was also observed also for carbon dioxide (CO_2) content in the Li-mediated PEC NRR performance (Figure S19, Supporting Information). This is because the exposure of Li_3N to CO_2 led to the formation of stable Li_2CO_3, enhancing the Li-mediated PEC NRR performance in a similar manner as that for O_2.

To demonstrate the potential use of the Si-based hierarchically-structured $PdCu/TiO_2/Si$ photocathode, we also performed the stability test. As shown in Figure S20 (Supporting Information), the Li-mediated PEC NRR cell based on the $PdCu/TiO_2/Si$ photocathode displayed little photocurrent decay over 20 h operation with a linear increase in the NH_3 yield and an almost constant FE (Figure S21, Supporting Information). Meanwhile, on the basis of five cyclic measurements of Li-mediated PEC NRR (Figure S22, Supporting Information), the PEC properties (such as photocurrent density) and synthetic behavior of NH_3 (such as NH_3 yield rate and FE) of $PdCu/TiO_2/Si$ photocathode are almost identical, implying that the photocathode owns a good durability. Its good stability and photosensitivity were also evidenced by the repeatable photocurrent responses from the $PdCu/TiO_2/Si$ photocathode in the electrolyte containing 3% O_2 under 4-MPa pressure at 0.07 V versus $Li^{0/+}$ while chopping the light at interval time of 1 h (Figure S23, Supporting Information). Clearly, the newly-developed Li-mediated PEC NRR cell can provide an efficient and stable route for the green synthesis of NH_3.

Finally, we performed the high sensitivity and nondestructive quasi in situ electron paramagnetic resonance (EPR) spectroscopy to detect chemical states of the materials in the SEI layer and unravel the enhanced catalytic performance. To maintain the original state of the SEI layer after PEC NRR, a

thin electrolyte layer was coated on the surface of $PdCu/TiO_2$/Si to avoid the air oxidation prior to the EPR measurements. As shown in Figure 4c, a sharp EPR signal at $\approx g_{\perp} = 1.966$, corresponding to the presence of metallic Li with unpaired electron,[45] is evident for all the photocathodes after the Li-mediated PEC NRR with different proton sources. The EPR signal intensity is closely related to the content of metallic Li in the SEI layer (the EPR tests conducted in the study were corrected using internal reference). Specifically, the EPR intensity for the metallic Li is inversely proportional to the Bronsted acidity of the proton donor in the electrolyte (Figure 4c), indicating, once again, that the proton donor with a stronger Bronsted acidity has ruptured more Li–N bonds to accelerate the NH_3 formation and move the cycle (II) in Figure 4a further forward, and hence the reduced Li content. Similar EPR intensity changes were also observed for the $PdCu/TiO_2$/Si photocathode after the Li-mediated PEC NRR under the N_2/O_2 mixture gas with different O_2 concentrations (Figure S24, Supporting Information). According to the previous publication,[21] however, more efficient Li-mediated NRR is usually observed for the photocathode with more Li/Li_3N to start with. Actually, stronger EPR signal of metallic Li (see Figure S25 in the Supporting Information) was found on the photocathode surface after PEC NRR under higher N_2 pressure, consistent with the higher NH_3 production rate and higher FE, when the formation of Li_3N was determining step. Figure 4d summaries the effects of various factors on the Li-mediated PEC NRR process investigated in this study. As can be seen, the more metallic Li materials are easily obtained on the active PdCu sites in the $PdCu/TiO_2$/Si photocathode, compared to the inert surface (e.g., TiO_2/Si), which is favorable for the first step of the Li-mediated PEC NRR: $Li^+ + e^- \rightarrow Li$. The NRR process is then limited for the second step of the Li_3N formation due to the low N_2 solubility despite the presence of sufficient metallic Li on the photocathode surface. The application of pressure to increase the N_2 solubility in the electrolytes can remarkably facilitate the formation of Li_3N, leading to the plentiful Li_3N on the photocathode surface. As a result, the increased Li_3N by increasing the N_2 pressure can overcome the second rate-limiting step of the Li-mediated PEC NRR ($6Li + N_2 \rightarrow 2Li_3N$) to obtain a high NH_3 yield rate and FE until over the optimal value of Li_3N. When the Li_3N is excessive, the relatively slow rate for the decomposition/hydrogenation of Li_3N ($Li_3N + 3H^+ \rightarrow 3Li^+ + NH_3$) becomes the rate-determining step to hinder the Li-mediated PEC NRR. To accelerate the NH_3 synthesis and Li cycle, the introduction of strong proton donors and O_2/CO_2 can enhance the rupture of the Li–N bonds and facilitate the formation of the N–H bonds. For an ideal Li-mediated PEC NRR process, these three steps in the Li cycle (Figure 2c) complements each other with an overall fast reaction rate.

3. Conclusion

In this study, we have developed a highly-efficient solar-powered, Li-mediated PEC NRR process for direct conversion of N_2-to-NH_3 with a remarkably high NH_3 yield rate (43.09 μg cm^{-2} h^{-1}) and faradaic efficiency (46.15%). Through comprehensive operando characterization, we, for the first time, have also gained a detailed mechanistic understanding on the Li-mediated PEC NRR process using the Si-based hierarchically-structured $PdCu/TiO_2$/Si photocathode. The results indicate that the formation and decomposition/hydrogenation of Li_3N are the rate-limiting steps for the Li-mediated PEC NRR, which can be effectively regulated by controlling the reaction conditions, including the N_2 pressure, nature of the proton sources, and introduction of oxidizing gases such as O_2 and CO_2. This work provides a new and systematic approach towards rational design and development of Li-mediated PEC NRR systems for fast, cost-effective, and efficient green synthesis of NH_3.

Supporting Information

Supporting Information is available from the Wiley Online Library or from the author.

Acknowledgements

The authors are grateful to the National Natural Science Foundation of China (22075075), the Key R&D Program of China (2021YFA1500900), the Outstanding Youth Scientist Foundation of Hunan Province (2022JJ10023), the Hunan Province of Huxiang Talent project (2021RC3051), the Provincial Natural Science Foundation of Hunan (2021JJ40140), the Research Foundation of Education Bureau of Hunan Province (21B0812) and Australian Research Council (DP180100568, DP180100731, DP190103881, and FL190100126) for financial support of this research.

Open access publishing facilitated by Curtin University, as part of the Wiley - Curtin University agreement via the Council of Australian University Librarians.

Conflict of Interest

The authors declare no conflict of interest.

Author Contributions

X.Z., Y.L., and H.Z. contributed equally to this work. J.Z. conceived the ideas, designed the research, and oversaw the entire project. X.Z. and Y.L. synthesized and characterized the photocathodes, conducted photoelectrochemical measurements and analyzed the data. H.Z. and A.H. implemented the XRD, Raman and FESEM measurements. J.D. and C.X. assisted X.Z. to complete EPR testing. H.Z., R.D.M., N.T., and V.K. carried out the SR-XPS measurements and data analysis. X.Z., J.Z., S.P.J, L.D., and S.Y.W co-wrote the paper and provided intellectual input to the manuscript.

Data Availability Statement

The data that support the findings of this study are available in the supplementary material of this article.

Keywords

photoelectrochemical nitrogen reduction reaction, lithium-mediated nitrogen reduction reaction, N_2-to-NH_3 fixation, reaction mechanism

Received: December 19, 2022
Revised: February 16, 2023
Published online: March 30, 2023

[1] M. J. Chalkley, M. W. Drover, J. C. Peters, *Chem. Rev.* **2020**, *120*, 5582.
[2] M.-M. Shi, D. Bao, B.-R. Wulan, Y.-H. Li, Y.-F. Zhang, J.-M. Yan, Q. Jiang, *Adv. Mater.* **2017**, *29*, 1606550.
[3] C. Negri, T. Selleri, E. Borfecchia, A. Martini, K. A. Lomachenko, T. V. W. Janssens, M. Cutini, S. Bordiga, G. Berlier, *J. Am. Chem. Soc.* **2020**, *142*, 15884.
[4] Y. Fang, Z. Liu, J. Han, Z. Jin, Y. Han, F. Wang, Y. Niu, Y. Wu, Y. Xu, *Adv. Energy Mater.* **2019**, *9*, 1803406.
[5] K. Peramaiah, V. Ramalingam, H.-C. Fu, M. M. Alsabban, R. Ahmad, L. Cavallo, V. Tung, K.-W. Huang, J.-H. He, *Adv. Mater.* **2021**, *33*, 2100812.
[6] H. E. Kim, J. Kim, E. C. Ra, H. Zhang, Y. J. Jang, J. S. Lee, *Angew. Chem., Int. Ed.* **2022**, *61*, e202204117.
[7] J. Zheng, L. Jiang, Y. Lyu, S. P. Jiang, S. Wang, *Energy Environ. Mater.* **2022**, *5*, 452.
[8] Y. Tong, H. Guo, D. Liu, X. Yan, P. Su, J. Liang, S. Zhou, J. Liu, G. Q. Lu, S. X. Dou, *Angew. Chem., Int. Ed.* **2020**, *59*, 7356.
[9] N. Zhang, F. Zheng, B. Huang, Y. Ji, Q. Shao, Y. Li, X. Xiao, X. Huang, *Adv Mater* **2020**, *32*, 1906477.
[10] J. Zheng, Y. Lyu, M. Qiao, J. P. Veder, R. D. Marco, J. Bradley, R. Wang, Y. Li, A. Huang, S. P. Jiang, S. Wang, *Angew. Chem.* **2019**, *58*, 18604.
[11] J. Zheng, Y. Lyu, M. Qiao, R. Wang, Y. Zhou, H. Li, C. Chen, Y. Li, H. Zhou, S. P. Jiang, S. Wang, *Chem* **2019**, *5*, 617.
[12] Z.-H. Xue, S.-N. Zhang, Y.-X. Lin, H. Su, G.-Y. Zhai, J.-T. Han, Q.-Y. Yu, X.-H. Li, M. Antonietti, J.-S. Chen, *J. Am. Chem. Soc.* **2019**, *141*, 14976.
[13] M. Wang, S. Liu, H. Ji, T. Yang, T. Qian, C. Yan, *Nat. Commun.* **2021**, *12*, 3198.
[14] J. Zheng, Y. Lyu, A. Huang, B. Johannessen, X. Cao, S. P. Jiang, S. Wang, *Chin. J. Catal.* **2023**, *45*, 141.
[15] J. Zheng, Y. Lyu, J.-P. Veder, B. Johannessen, R. Wang, R. De Marco, A. Huang, S. P. Jiang, S. Wang, *J. Phys. Chem. C* **2021**, *125*, 23041.
[16] F. Zhou, L. M. Azofra, M. Ali, M. Kar, A. N. Simonov, C. McDonnell-Worth, C. Sun, X. Zhang, D. R. MacFarlane, *Energy Environ. Sci.* **2017**, *10*, 2516.
[17] B. H. R. Suryanto, K. Matuszek, J. Choi, R. Y. Hodgetts, H.-L. Du, J. M. Bakker, C. S. M. Kang, P. V. Cherepanov, A. N. Simonov, D. R. MacFarlane, *Science* **2021**, *372*, 1187.
[18] L.-F. Gao, Y. Cao, C. Wang, X.-W. Yu, W.-B. Li, Y. Zhou, B. Wang, Y.-F. Yao, C.-P. Wu, W.-J. Luo, Z.-G. Zou, *Angew. Chem., Int. Ed.* **2021**, *60*, 5257.
[19] S. Li, Y. Zhou, K. Li, M. Saccoccio, R. Sažinas, S. Z. Andersen, J. B. Pedersen, X. Fu, V. Shadravan, D. Chakraborty, J. Kibsgaard, P. C. K. Vesborg, J. K. Nørskov, I. Chorkendorff, *Joule* **2022**, *6*, 2083.
[20] H.-L. Du, M. Chatti, R. Y. Hodgetts, P. V. Cherepanov, C. K. Nguyen, K. Matuszek, D. R. MacFarlane, A. N. Simonov, *Nature* **2022**, *609*, 722.
[21] S. Z. Andersen, M. J. Statt, V. J. Bukas, S. G. Shapel, J. B. Pedersen, K. Krempl, M. Saccoccio, D. Chakraborty, J. Kibsgaard, P. C. K. Vesborg, J. Nørskov, I. Chorkendorff, *Energy Environ. Sci.* **2020**, *13*, 4291.
[22] K. Li, S. G. Shapel, D. Hochfilzer, J. B. Pedersen, K. Krempl, S. Z. Andersen, R. Sažinas, M. Saccoccio, S. Li, D. Chakraborty, J. Kibsgaard, P. C. K. Vesborg, J. K. Nørskov, I. Chorkendorff, *ACS Energy Lett.* **2022**, *7*, 36.
[23] C. Chen, X. Zhu, X. Wen, Y. Zhou, L. Zhou, H. Li, L. Tao, Q. Li, S. Du, T. Liu, D. Yan, C. Xie, Y. Zou, Y. Wang, R. Chen, J. Huo, Y. Li, J. Cheng, H. Su, X. Zhao, W. Cheng, Q. Liu, H. Lin, J. Luo, J. Chen, M. Dong, K. Cheng, C. Li, S. Wang, *Nat. Chem.* **2020**, *12*, 717.
[24] J. Zheng, S. Bao, X. Zhang, H. Wu, R. Chen, P. Jin, *Appl. Catal., B* **2016**, *183*, 69.
[25] J. Zheng, Y. Lyu, C. Xie, R. Wang, L. Tao, H. Wu, H. Zhou, S. Jiang, S. Wang, *Adv. Mater.* **2018**, *30*, 1801773.
[26] B. H. R. Suryanto, H. L. Du, D. B. Wang, J. Chen, A. N. Simonov, D. R. MacFarlane, *Nat. Catal.* **2019**, *2*, 290.
[27] N. Lazouski, Z. J. Schiffer, K. Williams, K. Manthiram, *Joule* **2019**, *3*, 1127.
[28] H. Cheng, P. Cui, F. Wang, L.-X. Ding, H. Wang, *Angew. Chem., Int. Ed.* **2019**, *58*, 15541.
[29] J. A. Schwalbe, M. J. Statt, C. Chosy, A. R. Singh, B. A. Rohr, A. C. Nielander, S. Z. Andersen, J. M. McEnaney, J. G. Baker, T. F. Jaramillo, J. K. Norskov, M. Cargnello, *ChemElectroChem* **2020**, *7*, 1542.
[30] Q. Fu, A. Sarapulova, V. Trouillet, L. Zhu, F. Fauth, S. Mangold, E. Welter, S. Indris, M. Knapp, S. Dsoke, N. Bramnik, H. Ehrenberg, *J. Am. Chem. Soc.* **2019**, *141*, 2305.
[31] Y. S. Zhou, F. L. Che, M. Liu, C. Q. Zou, Z. Q. Liang, P. De Luna, H. F. Yuan, J. Li, Z. Q. Wang, H. P. Xie, H. M. Li, P. N. Chen, E. Bladt, R. Quintero-Bermudez, T. K. Sham, S. Bals, J. Hofkens, D. Sinton, G. Chen, E. H. Sargent, *Nat. Chem.* **2018**, *10*, 974.
[32] J. Y. Zheng, S. H. Bao, Y. Guo, P. Jin, *ACS Appl. Mater. Interfaces* **2014**, *6*, 1351.
[33] N. J. Divins, A. Braga, X. Vendrell, I. Serrano, X. Garcia, L. Soler, I. Lucentini, M. Danielis, A. Mussio, S. Colussi, I. J. Villar-Garcia, C. Escudero, A. Trovarelli, J. Llorca, *Nat. Commun.* **2022**, *13*, 5080.
[34] Y. Qiao, H. Yang, Z. Chang, H. Deng, X. Li, H. Zhou, *Nat. Energy* **2021**, *6*, 653.
[35] J. Du, W. Wang, A. Y. Sheng Eng, X. Liu, M. Wan, Z. W. Seh, Y. Sun, *Nano Lett.* **2020**, *20*, 546.
[36] Y. Luo, T. Li, H. Zhang, W. Liu, X. Zhang, J. Yan, H. Zhang, X. Li, *Angew. Chem., Int. Ed.* **2021**, *60*, 11718.
[37] G.-F. Chen, A. Savateev, Z. Song, H. Wu, Y. Markushyna, L. Zhang, H. Wang, M. Antonietti, *Angew. Chem., Int. Ed.* **2022**, *61*, e202203170.
[38] G. G. Eshetu, X. Judez, C. Li, O. Bondarchuk, L. M. Rodriguez-Martinez, H. Zhang, M. Armand, *Angew. Chem., Int. Ed.* **2017**, *56*, 15368.
[39] V. S. Patil, K. Vithya, M. Premalatha, B. Sundaresan, *Macromol. Symp.* **2019**, *387*, 1800177.
[40] N. Ahmad, S. Sun, P. Yu, W. Yang, *Adv. Funct. Mater.* **2022**, *32*, 2201528.
[41] F. Pan, K. Ni, Y. Ma, H. Wu, X. Tang, J. Xiong, Y. Yang, C. Ye, H. Yuan, M.-L. Lin, J. Dai, M. Zhu, P.-H. Tan, Y. Zhu, K. S. Novoselov, *Nano Lett.* **2021**, *21*, 5648.
[42] D. Lee, S. Sun, J. Kwon, H. Park, M. Jang, E. Park, B. Son, Y. Jung, T. Song, U. Paik, *Adv. Mater.* **2020**, *32*, 1905573.
[43] Z. Chen, W. Chen, H. Wang, C. Zhang, X. Qi, L. Qie, F. Wu, L. Wang, F. Yu, *Nano Energy* **2022**, *93*, 106836.
[44] K. Li, S. Z. Andersen, M. J. Statt, M. Saccoccio, V. J. Bukas, K. Krempl, R. Sažinas, J. B. Pedersen, V. Shadravan, Y. Zhou, D. Chakraborty, J. Kibsgaard, P. C. K. Vesborg, J. K. Nørskov, I. Chorkendorff, *Science* **2021**, *374*, 1593.
[45] M. J. N. Junk, W. Li, A. D. Schlüter, G. Wegner, H. W. Spiess, A. Zhang, D. Hinderberger, *Angew. Chem., Int. Ed.* **2010**, *49*, 5683.